



OPEN

Parametric simulation of micropolar fluid with thermal radiation across a porous stretching surface

Muhammad Bilal¹, Anwar Saeed², Taza Gul¹, Wiyada Kumam³✉, Safyan Mukhtar⁴ & Poom Kumam^{2,5}✉

The energy transmission through micropolar fluid have a broad range implementation in the field of electronics, textiles, spacecraft, power generation and nuclear power plants. Thermal radiation's influence on an incompressible thermo-convective flow of micropolar fluid across a permeable extensible sheet with energy and mass transition is reported in the present study. The governing equations consist of Navier–Stokes equation, micro rotation, temperature and concentration equations have been modeled in the form of the system of Partial Differential Equations. The system of basic equations is reduced into a nonlinear system of coupled ODE's by using a similarity framework. The numerical solution of the problem has been obtained via PCM (Parametric Continuation Method). The findings are compared to a MATLAB built-in package called *bvp4c* to ensure that the scheme is valid. It has been perceived that both the results are in best agreement with each other. The effects of associated parameters on the dimensionless velocity, micro-rotation, energy and mass profiles are discussed and depicted graphically. It has been detected that the permeability parameter gives rise in micro-rotation profile.

Abbreviations

x, y	Velocity component
$U_0 = bx$	Stretching velocity
Δ	Coupling parameter
Nr	Inertia coefficient
M	Permeability parameter
Sc	Schmidt number
R	Thermal radiation
Pr	Prandtl number
Sr	Soret number
G	Microrotation parameter
Du	Dufour number
Cf	Skin friction
Nu_x	Nusselt number
Sh_x	Sherwood number
Re	Reynold number
PCM	Parametric continuation method
BVP	Boundary value problem

¹Department of Mathematics, City University of Science and Information Technology, Peshawar 25000, Pakistan. ²Present address: Center of Excellence in Theoretical and Computational Science (TaCS-CoE), Faculty of Science, King Mongkut's University of Technology Thonburi (KMUTT), 126 Pracha Uthit Rd., Bang Mod, Thung Khru, Bangkok 10140, Thailand. ³Present address: Applied Mathematics for Science and Engineering Research Unit (AMSERU), Program in Applied Statistics, Department of Mathematics and Computer Science, Faculty of Science and Technology, Rajamangala University of Technology Thanyaburi (RMUTT), Pathum Thani 12110, Thailand. ⁴Department of Basic Sciences, Deanship of Preparatory Year, King Faisal University, Al Ahsa, Hofuf, Saudi Arabia. ⁵Department of Medical Research, China Medical University Hospital, China Medical University, Taichung 40402, Taiwan. ✉email: wiyada.kum@rmutt.ac.th; poom.kum@kmutt.ac.th

PDE	Partial differential equation
ODE	Ordinary differential equation
$f(\eta), g(\eta)$	Dimensionless velocity
$\phi(\eta)$	Dimensionless concentration
$\theta(\eta)$	Dimensionless temperature
bvp4c	Matlab built-in package

The transfer of heat along thin film flow of micropolar fluid has a great impact on research in the field of electronics and especially the exchange of heat inside the circuits of electronic devices, due to uncountable applications described in¹. To maximize and improve the allowance of heat transfer of patterns flow, extension in the surface flow has been highly effective. Heat transmission is extremely important in industries such as vehicles, textiles, and machines, as well as in the design of all industrial equipment, such as jets, army emanations, spacecraft, turbines of various power generation, and nuclear power plants². To examine the impacts of radiations on the boundary layer of fluids is not an easy job to deal. The phenomenon of heat transfer was explained by Cengel³, in the encyclopedia of energy engineering and technology. Khoshvaght et al.⁴ explored the dynamics of flow and heat exchange on Sinusoidal-Corrugated tubes computationally. The Micro polar fluid was first introduced by Eringe⁵, who explains the micro-rotation effects on the micro-structures because the theory presented by Navier and Stokes does not explain, precisely the properties associated with polymeric fluids, colloidal fluids, suspension and solutions, liquids containing crystals and fluids with additives. Stokes⁶ presented a theoretical approach to fluid flow with micro characteristics. Researchers are studying the effects of radiations on boundary layer of fluids over plates, The thermal radiations effect on micropolar conducting fluid across a uniform expanding surface is reported by Abo-Eldahab et al.⁷. Micropolar fluids with heat transition across a permeable medium under the consequences of radiations are discussed by Abo-Eldahab⁸. Ramesh et al.⁹ used chemical processes and activation energy effects to transmit the flow, heat, and mass transfer characteristics of a hybrid nanofluid across parallel surfaces. The consequences of viscous resistance on the boundary of the flow, with inertia force and heat transfer in a constant porosity was addressed by Reddy et al.¹⁰. Jyothi et al.¹¹ and Kumar et al.¹² examined the free convective flow of Maxwell nanofluid across a stretched sheet. The skin friction factor for the Maxwell component is larger than for the Newtonian fluid, and the local Nusselt number is lower for linear radiation and higher for non-linear radiation. Soundalgekar et al.¹³ explains the stream and exchange of warm over a ceaselessly moving plate. Gorla et al.¹⁴ investigated the steady heat propagation in micro polar fluid using similarity techniques. The convection micropolar fluid flow and heat propagation characteristics over a vertical surface are studied by Rees et al.¹⁵. Giresha & Ramesh¹⁶ used the Runge-Kutta-Fehlberg order approach to analyse the heat of a generalised Burgers nanofluid over a stretched sheet. Ramesh et al.¹⁷ investigated the dusty fluid's 2D boundary layer flow across a stretched sheet. The rate of heat transmission is calculated and presented for a variety of parameter values.

Electromagnetic radiation known as thermal radiation is in the wavelength range of 0.1 to 100 μm produced by all matter at a non-zero temperature. It covers a portion of the ultraviolet spectrum as well as all infrared and visible light. At elevated heat (over 1000 K) and following material implosion, when some objects are in clear view of heated debris situated below, radiation heat transmission across parallel sheets becomes significant. Because there aren't any suitable radiative heat exchange models, the energy transition across the plates will be inaccurate¹⁸. Mahanthesh and Mackolil¹⁹ investigate the heat propagation of a nanofluid over a plate surface by using quadratic thermal radiation. According to the findings, the density variation with energy differences has huge importance in thermal processes such as solar collectors. Kumar et al.²⁰ utilised a computational model that included thermal radiation, magnetic field and viscous dissipation to simulate the heat transmission and nanofluid flow along vertical infinite plate. It was realized that improving the value of the radiation constant enriches the energy and velocity profiles. Khader and Sharma²¹ examined the effects of non-uniform heat source and thermal radiation on MHD micropolar fluid flow over a shirking sheet. It has been discovered that the increment in thermal radiation coefficient and micro-polar constant enhances the fluid velocity.

Complex boundary value equations that cannot be resolved are common in the engineering industries. For many systems that are routinely addressed by other computational models, convergence is susceptible to the relaxation constants and starting strategy. The PCM's objective is to investigate the method's universal applicability as a sustainable solution to nonlinear issues²². The 3D irregular fluid and heat dispersion over the surface of a rough stretchy spinning disc was highlighted by Shuaib et al.²³. In addition to the influence of external magnetic field, the fluid has been investigated. Shuaib et al.²⁴ found the property of an ionic transitional boundary layer flow across a revolving disc. Wang et al.²⁵ Khan reported a parametric continuation algorithm-based stability assessment of nonlinear systems for engineering disciplines. They also investigated the bifurcation that occurs while solving nonlinear IVPs with distinct features and developed an algorithm for determining the bifurcation points in real time.

In our study, we explored the heat exchange in a micropolar fluid with the impacts of radiation across a permeable medium. The problem has been arranged in the form of PDEs (Navier Stokes, energy and concentration equation). The PDEs system has been diminished into the system of ODEs using similarity framework. Which are numerically solved via PCM technique. For this purpose, the modeled equations are tackled numerically by using two different numerical techniques, predictor corrector method and bvp4c method. The obtained conclusions are compared and discussed with the help of graphs, which shows reasonable settlement with each other.

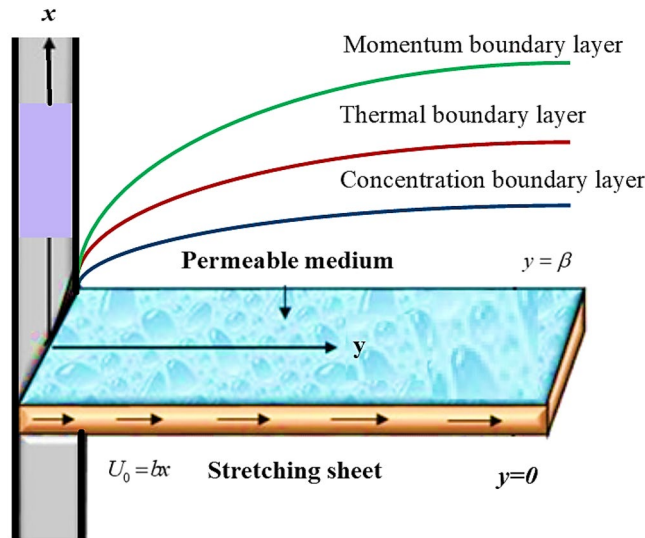


Figure 1. The fluid flow over a stretching surface.

Mathematical formulation

Considered the micropolar fluid flow across a stretched plate with velocity $U_0 = bx$. The uniform stretching rate is specified by $b > 0$, along the x -direction. Let d , be the thickness of the surface. The medium is assumed to be permeable over an infinite horizontal sheet in the region $y > 0$ as illustrated in Fig. 1. The thermal radiations effect has been considered along an x -coordinate. Under the above-mentioned presumptions, the flow problem in the of PDEs can be stated as^{26,27,29}:

$$\frac{\partial u}{\partial x} + \frac{\partial v}{\partial y} = 0, \tag{1}$$

$$u \frac{\partial u}{\partial x} + v \frac{\partial u}{\partial y} = \nu \frac{\partial^2 u}{\partial y^2} + k_c \frac{\partial \sigma}{\partial y} + \frac{\nu \varphi}{K} (U - u) + C_r \varphi (U^2 - u^2), \tag{2}$$

$$G_1 \frac{\partial^2 \sigma}{\partial y^2} - 2\sigma - \frac{\partial u}{\partial y} = 0, \tag{3}$$

$$u \frac{\partial \tau}{\partial x} + v \frac{\partial \tau}{\partial y} = \frac{k}{\rho c_p} \frac{\partial^2 \tau}{\partial y^2} + \frac{16\sigma^*}{3\rho c_p k^*} \frac{\partial^2 \tau}{\partial y^2} + \frac{\nu D_m k_T}{T_m c_s c_p} \frac{\partial^2 C}{\partial y^2}, \tag{4}$$

$$u \frac{\partial C}{\partial x} + v \frac{\partial C}{\partial y} = D_m u \frac{\partial^2 C}{\partial y^2} + \frac{D_m k_T}{T_m} \frac{\partial^2 \tau}{\partial y^2}. \tag{5}$$

Boundary conditions for the two-dimensional flow is given as^{26,27}:

$$\left. \begin{aligned} u = U_0, \quad v = 0, \quad \sigma = 0, \quad \tau = \tau_w, \quad C = C_w \quad \text{at } y = 0, \\ u_y = \sigma_y = \tau_y = C_y = 0, \quad v = \delta_x \quad \text{at } y \rightarrow 0, \end{aligned} \right\} \tag{6}$$

Here, the thermal radiation term is defined as:

$$q_r = \frac{4\sigma^*}{3K^*} \frac{\partial \tau^4}{\partial y}, \tag{7}$$

While, ignoring the higher order terms in Taylor's series, we consider only τ_4 about τ_1 , which can be expressed as:

$$\tau^4 \simeq 4\tau_1^3 \tau^* - 3\tau_1^4. \tag{8}$$

by using Eqs. (7) and (8), Eq. (4) becomes,

$$u \frac{\partial \tau}{\partial x} + v \frac{\partial \tau}{\partial y} = \frac{k}{\rho c_p} \frac{\partial^2 \tau}{\partial y^2} + \frac{16\sigma^* \tau_1^3}{3\rho c_p k^*} \frac{\partial^2 \tau}{\partial y^2} + \frac{v D_m k_T}{T_m c_s c_p} \frac{\partial^2 C}{\partial y^2}, \tag{9}$$

The corresponding similarity transformations are²⁶:

$$\begin{aligned} \psi(x, y) &= (2\nu U_0 x)^{\frac{1}{2}} f(\eta), \quad u = \psi_y, \quad v = -\psi_x, \\ \sigma &= \left(\frac{U_0}{2\nu x}\right)^{\frac{1}{2}} U_0 g(\eta) \quad \text{and} \quad \eta = \left(\frac{U_0}{2\nu x}\right)^{\frac{1}{2}} y. \end{aligned} \tag{10}$$

The temperature and concentration for the thin film flow are

$$\theta(\eta) = \left(\frac{\tau - \tau_\infty}{\tau_w - \tau_\infty}\right) \quad \text{and} \quad \phi(\eta) = \left(\frac{C - C_\infty}{C_w - C_\infty}\right). \tag{11}$$

In the consequences of Eq. (10) and Eq. (11) in Eqs. (1)–(6), we get:

$$f''' + \Delta g' + ff'' + \frac{1}{M}(1 - f') + (1 - f'^2) = 0, \tag{12}$$

$$Gr g'' - 2(2g + f'') = 0, \tag{13}$$

$$(4 + 3R)\theta'' + 3R Pr(Du\phi'' + f\theta') = 0, \tag{14}$$

$$\phi'' + Sr\theta'' - Scf\phi' = 0. \tag{15}$$

The system of ODEs transforms boundary conditions are:

$$\left. \begin{aligned} f(0) = g(0) = f(0) = \theta(0) = \phi(0) = 1 \quad \text{at} \quad y = 0 \\ f'(1) = f(1) = g'(1) = \theta'(1) = \phi'(0) = 0 \quad \text{at} \quad y = 1. \end{aligned} \right\} \tag{16}$$

where, $\Delta = k_c/\nu$ is the coupling parameter, $Nr = 2\varphi C_r u_0/a$ is the inertia coefficient parameter, $M = ka/2\varphi\nu$ is the permeability parameter, $Gr = G_1 a/\nu$ denotes micro rotation parameter, $R = 4\sigma^* \tau_1^3/K^*$ denotes radiations parameter, $Pr = \rho\nu c_p/k$ denotes Prandtl number, $Sc = \nu/D_m$ denotes Schmidt number, $Sr = D_m K_T(T_w - T_0)/\nu T_m(C_w - C_0)$ denotes Soret number and $Du = D_m K_T(C_w - C_0)/\nu T_m(T_w - T_0)$ denotes Dufour number.

The drag force, Nusselt and Sherwood number, which have several physical and engineering interpretations, are determined as:

$$C_f = \frac{\tau_w^s}{\rho u_w^2}, \quad Nu_x = \frac{xq_w}{K(\tau_w - \tau_\infty)}, \quad Sh_x = \frac{xq_m}{D_m(C_w - C_\infty)}. \tag{17}$$

where τ_w^s, q_w and q_m are the shear stress, heat and mass fluctuation at the surface, which can be rebound as:

$$\tau_w^s = \mu \left(\frac{\partial u}{\partial y}\right)^{y=0}, \quad q_w = -\left(K \frac{\partial \tau}{\partial y}\right)^{y=0}, \quad q_m = -\left(D_m \frac{\partial C}{\partial y}\right)^{y=0}. \tag{18}$$

With μ being the dynamic viscosity, then from (17) and (18) into (17), we get

$$C_f Re_x^{\frac{1}{2}} = -f''(0), \quad Nu_x Re_x^{-\frac{1}{2}} = -\theta'(0), \quad Sh_x Re_x^{-\frac{1}{2}} = -\phi'(0). \tag{19}$$

Here $Re = \frac{u_0 x}{\nu}$ is Reynold number.

Solution procedures

In this section, the basic methodology and step wise solution of PCM technique have been expressed.

Step 1

We presented the following variables to reduced system of BVP to first order:

$$\zeta_1 = f, \quad \zeta_2 = f', \quad \zeta_3 = f'', \quad \zeta_4 = g, \quad \zeta_5 = g', \quad \zeta_6 = \theta, \quad \zeta_7 = \theta', \quad \zeta_8 = \phi, \quad \zeta_9 = \phi'. \tag{20}$$

Making use of Eq. (20) in Eqs. (12–15) and (16), we obtained:

$$\zeta_3' \Delta \zeta_5 + \zeta_1 \zeta_3 + \frac{1}{M}(1 - \zeta_4) + N(1 - \zeta_2^2) = 0, \tag{21}$$

$$Gr \zeta_5' 2(2\zeta_4 + \zeta_3) = 0, \tag{22}$$

$$(3R + 4)\zeta_7' - 3R \text{Pr}(Du\zeta_9' + \zeta_7\zeta_1) = 0, \quad (23)$$

$$\zeta_9' + Sr\zeta_7' - Sc\zeta_9\zeta_1 = 0. \quad (24)$$

The conditions for first order system of differential equations are:

$$\left. \begin{aligned} \zeta_1(0) = \zeta_2(0) = \zeta_4(0) = \zeta_6(0) = \zeta_8(0) = 1, \quad \text{at } y = 0, \\ \zeta_3(1) = \zeta_1(1) = \zeta_5(1) = \zeta_7(1) = \zeta_9(1) = 0, \quad \text{at } y = 1. \end{aligned} \right\} \quad (25)$$

Step 2 Introducing the parameter p in Eqs. (21–24):

$$\zeta_3'\Delta\zeta_5 + \zeta_1(\zeta_3 - 1)p + \frac{1}{M}(1 - \zeta_4) + N(1 - \zeta_2^2) = 0, \quad (26)$$

$$Gr\zeta_5'2(2\zeta_4 - \zeta_5 + (\zeta_5 - 1)p + \zeta_3) = 0, \quad (27)$$

$$(3R + 4)\zeta_7' - 3R \text{Pr}(Du\zeta_9' + (\zeta_7 - 1)p\zeta_1) = 0, \quad (28)$$

$$\zeta_9' + Sr\zeta_7' - Sc\zeta_1(\zeta_9 - 1)p = 0. \quad (29)$$

Step 3 Differentiating Eqs. (21–25) by parameter 'p'

$$V' = AV + R, \quad (30)$$

where, A and R is the coefficient matrix and the remainder.

$$\frac{d\zeta_i}{d\tau} \quad (31)$$

where $i = 1, 2, \dots, 11$.

Step 4 Apply superposition principle for each term

$$V = aU + W, \quad (32)$$

Solve the following two Cauchy problems for each term

$$U = aU, \quad (33)$$

$$W = AW + R, \quad (34)$$

introducing Eq. (32) in Eq. (30), we obtained

$$(aU + W)' = A(aU + W) + R, \quad (35)$$

Step 5 Solving the Cauchy problems

In order to solve the Cauchy issues, a numerical implicit approach is employed, as shown below from Eqs. (33) and (34)

$$\frac{U^{i+1} - U^i}{\Delta\eta} = AU^{i+1}, \quad \text{or } (I - \Delta\eta A)U^{i+1} = U^i, \quad (36)$$

$$\frac{W^{i+1} - W^i}{\Delta\eta} = AW^{i+1}, \quad \text{or } (I - \Delta\eta A)W^{i+1} = W^i, \quad (37)$$

from where we obtain the iterative form of the solution

$$U^{i+1} = (I - \Delta\eta A)^{-1}U^i, \quad (38)$$

$$W^{i+1} = (I - \Delta\eta A)^{-1}(W^i + \Delta\eta R). \quad (39)$$

Results and discussion

The thin film flow of micro-polar fluid in permeable media is investigated, as well as the combined influence of temperature and concentration fields across expands in plate. Distinct physical constraints upshot on velocity, energy and concentration profiles have been highlighted. The physical flow behavior is manifested through Fig. 1. Figure 2a evaluates the dependence of the coupling parameter Δ on the velocity $f(\eta)$. As can be seen, Δ is inversely linked to the kinematic viscosity of the fluid; as Δ grows, the thickness drops, and the velocity of the liquid rises.

Figure 2b depicts the effect of permeability Mr on the $f(\eta)$. Given that higher values for M resulting in a highly porous media, the fluid flow would obviously decelerate, leading to a drop in velocity. Figure 2c depicts

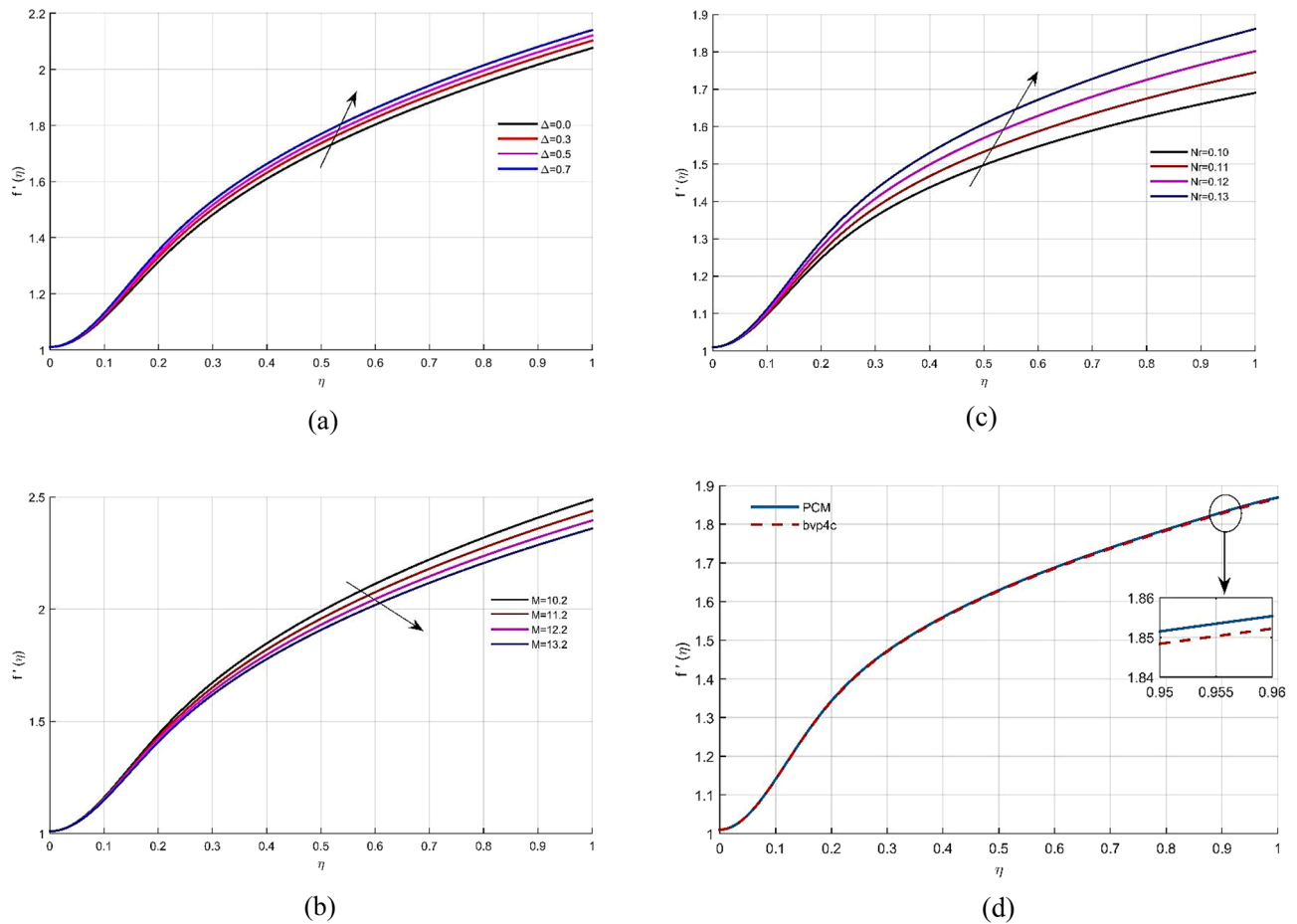


Figure 2. (a–d) The impact of Δ , Mr and Nr on non-dimensional velocity field $f'(\eta)$. (d) Comparison of solution obtained by PCM and bvp4c method.

the effect of the inertia coefficient Nr . It can be shown that boosting Nr credit increases fluid velocity. Figure 2d shows a comparative analysis of the PCM and bvp4c methods vs the velocity field $f(\eta)$. The micro-rotation circular velocity distribution $g(\eta)$ vs different physical constants is represented in Fig. 3a–d. The kinetic energy improves as the value of Gr (micro-rotation factor) rises. Physically, when the rotation parameter is elevated, the fluid’s kinematic viscosity drops, and fluid velocity rises. The consequence of the inertia component Nr on the radial velocity profile $g(\eta)$ is seen in Fig. 3b. The fluid velocity $g(\eta)$ declines as Nr increases. Figure 3c depicts the impact of the permeability element on the non-dimensional micro-rotation angular velocity. Because the permeability factor and the fluid’s viscosity are inversely related, as the permeability parameter increases, the viscosity lowers, and the radial velocity improves. Figure 3d illustrates the comparison of both strategies vs $g(\eta)$.

The temperature profile $\theta(\eta)$ of the fluid reduces with larger values of the radiation factor R , as illustrated in Fig. 4a, The rising effect of radiations reduces the fluid energy profile $\theta(\eta)$. Physically, a fluid with a high Prandtl number has a lower thermal diffusivity. The increase in Pr results in a reduction in $\theta(\eta)$ as displayed in Fig. 4b. Figure 4c shows that increasing the Schmidt number Sc lowers the thermal energy $\theta(\eta)$, because Schmidt number effect reduces the boundary layer thickness. The fluid temperature reduces with the action of Soret number Sr , as revealed through Fig. 4d. As a result, an enhancement in the Sr corresponds to rises in $\theta(\eta)$. Figure 4e shows the correlation between the Dufour number Du and energy profile. The fluid temperature enhances with the positive increment Dufour number Du . As demonstrated in Fig. 4f, both solutions for the temperature profile $\theta(\eta)$ have the best correlation.

Figure 5a explains the response of Sr on the concentration allocation $\phi(\eta)$. Because Soret number is directly related to viscosity. The upshot of Schmidt number Sc on concentration contour $\phi(\eta)$ is shown in Fig. 5b, which indicates that variation in Sc improves the concentration distribution. Figure 5c shows that when the Dufour number Du increases, the non-dimensional concentration profile of the liquid grows. As shown in Fig. 5d, the

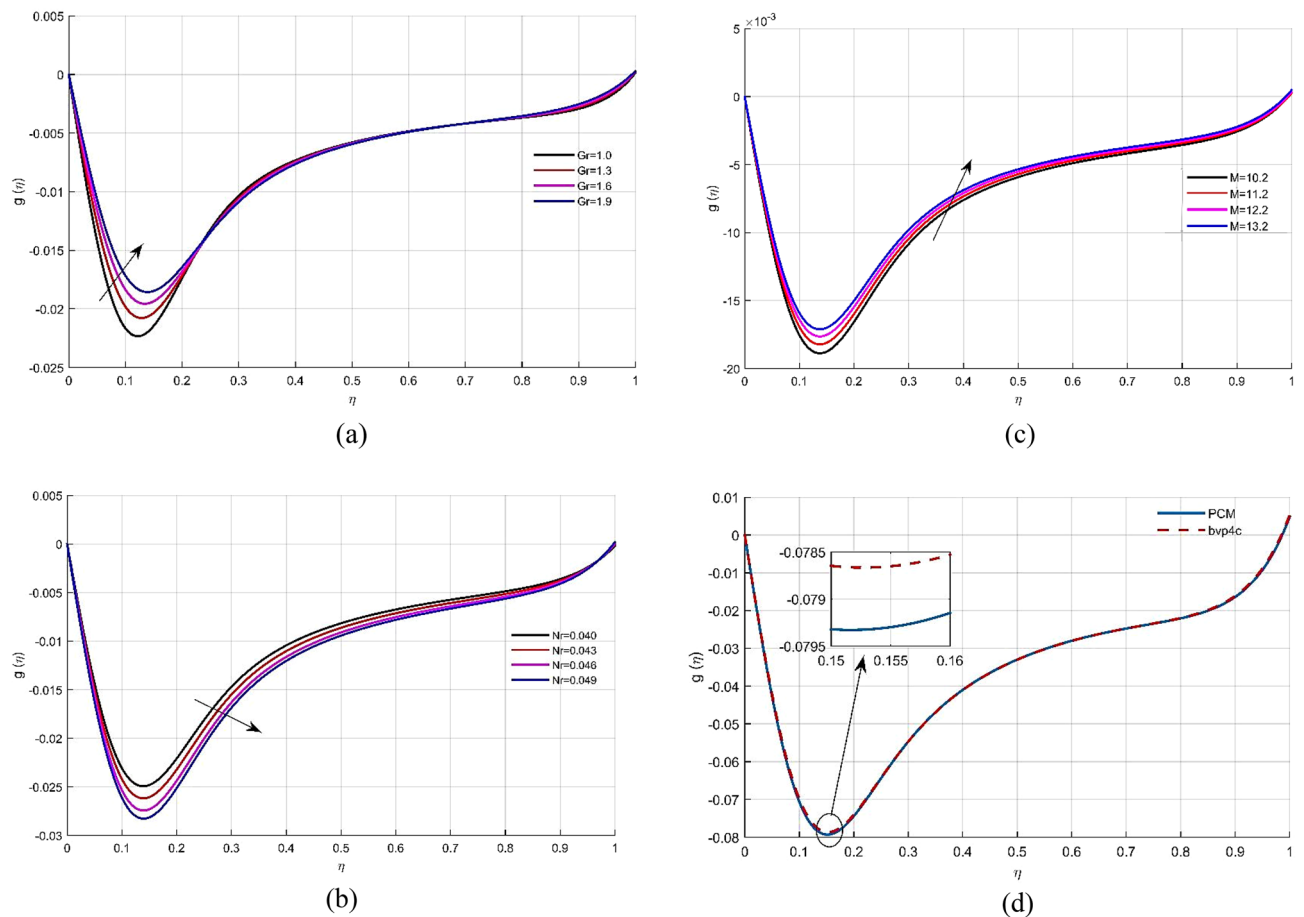


Figure 3. (a–d) Micro rotation profile $g(\eta)$ under the effects of Gr , Nr and Mr . (d) Comparison of solution obtained by PCM and bvp4c method.

numerical approximation for the concentration gradient $\phi(\eta)$ has the best agreement. Tables 1, 2, 3 provide the numerical results for skin friction, energy transmission, and Sherwood number, as well as a comparison to existing work. Tables 4 and 5 displays the computational estimates for axial velocity, energy, and mass transition profiles for the variation of embedded parameter values.

Conclusion

The mass and heat propagation through steady flow of micropolar fluid across a stretched permeable sheet have been analyzed. The modeled equations are numerically computed via PCM technique. The findings are verified with a Matlab source code called bvp4c to ensure that the outputs are accurate. Physical constraints have been explored in relation to velocity, temperature and concentration profiles. The following conclusion may be formed based on the findings of the aforementioned study:

- The PCM and bvp4c approaches are thought to be particularly efficient and reliable
- in determining numerical solutions for a wide range of nonlinear systems of partial differential equations.
- The permeability parameter M controls the mobility of the fluid particles, which result in lowering its velocity.
- The thermal radiation and Prandtl number show positive effect on the fluid temperature.
- With increasing credit of Schmidt number Sc , the thermal energy profile improves but the mass transmission rate reduces.
- The coefficient of skin friction rises when the radiation parameter and permeability parameter are elevated.

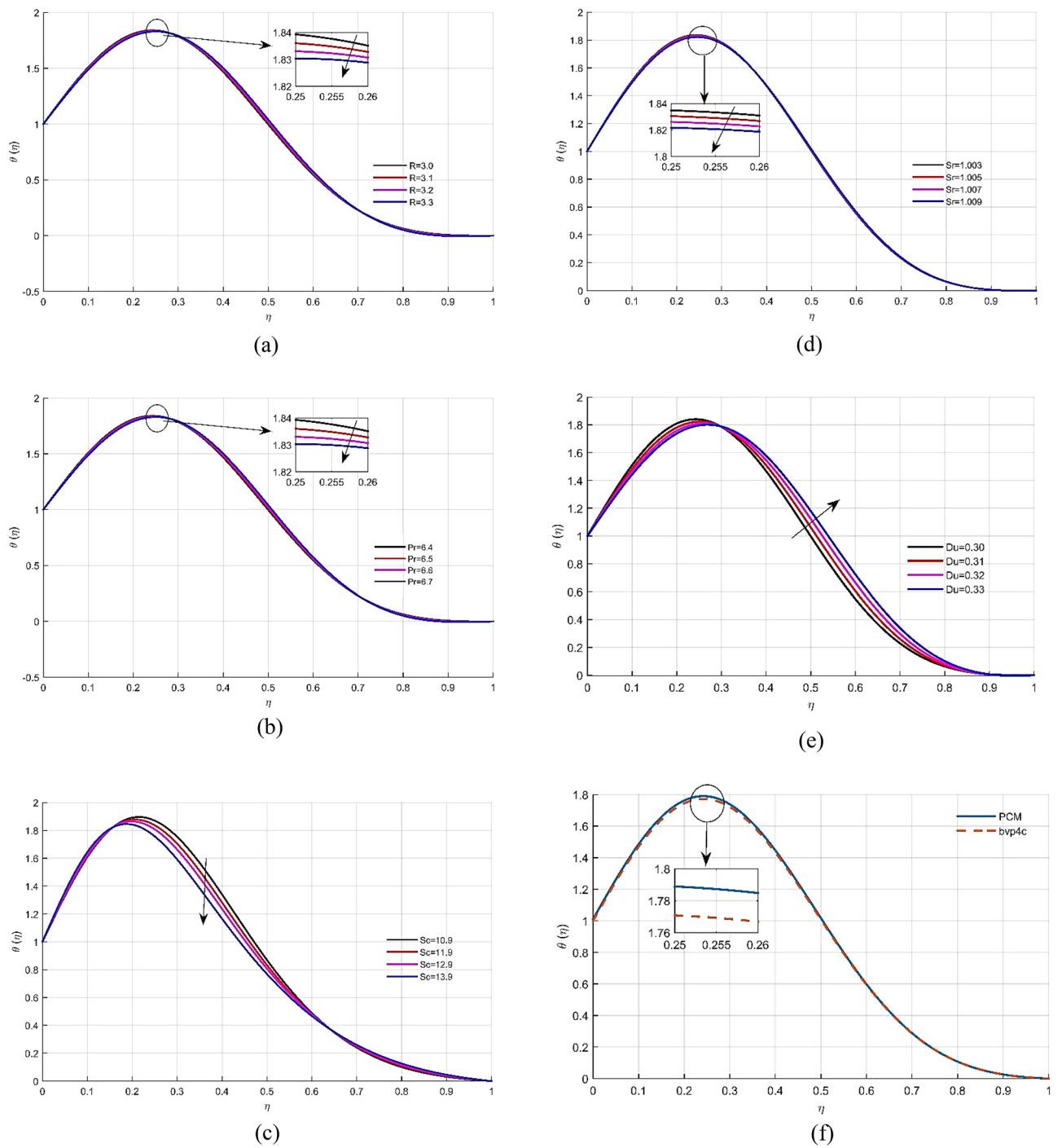


Figure 4. (a–f) Variation of dimensionless temperature profile $\theta(\eta)$ with parameters Rd , Pr , Sc , Sr and Du respectively. (f) Comparison of solution obtained by PCM and bvp4c method.

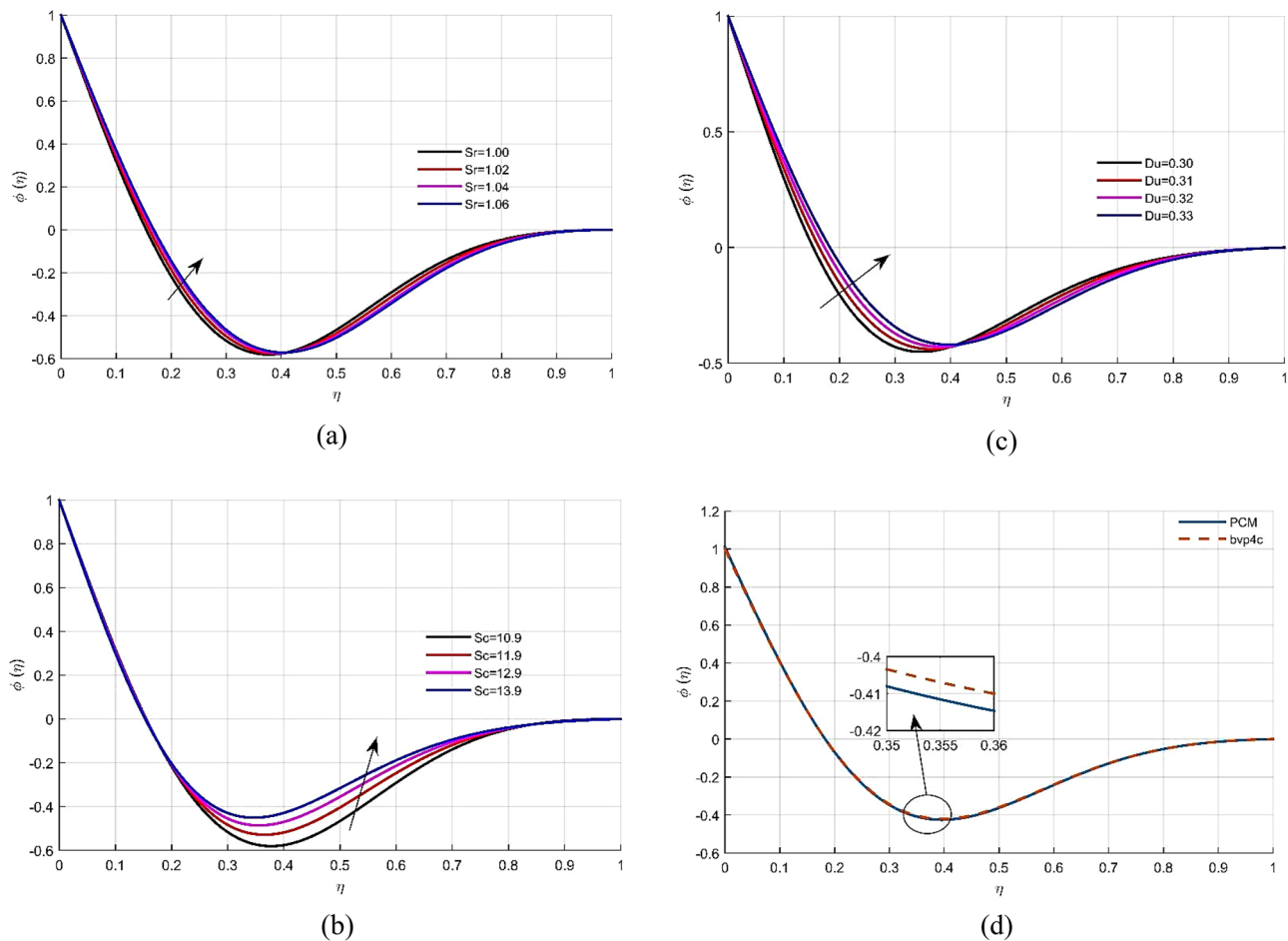


Figure 5. (a–d) The effects of parameters Sc , Sr and Du on dimensional less concentration profile $\phi(\eta)$ respectively. (d) Comparison of solution obtained by PCM and bvp4c method.

Δ	Mr	Nr	$(C_f)^{28}$	Δ	Mr	Nr	(C_f)
0.2	0.7	0.2	1.37594	0.2	0.7	0.2	1.37589
0.3	0.7	0.2	1.37571	0.3	0.7	0.2	1.37568
0.4	0.7	0.2	1.37547	0.4	0.7	0.2	1.37551
0.2	0.7	0.2	1.37594	0.2	0.7	0.2	1.37587
0.2	0.8	0.2	1.25938	0.2	0.8	0.2	1.25921
0.2	0.9	0.2	1.16533	0.2	0.9	0.2	1.16511
0.2	0.7	0.2	1.37594	0.2	0.7	0.2	1.37575
0.2	0.7	0.3	1.46338	0.2	0.7	0.3	1.46366
0.2	0.7	0.4	1.55067	0.2	0.7	0.4	1.55053

Table 1. Numerical outcomes for skin friction.

R	Pr	Nu_x^{28}	R	Pr	Nu_x
0.3	0.7	0.245742	0.3	0.7	0.245756
0.3	0.7	0.241842	0.3	0.7	0.241852
0.3	0.7	0.234106	0.3	0.7	0.234108
0.3	0.7	0.245742	0.3	0.7	0.245746
0.3	0.7	0.324886	0.3	0.7	0.324890
0.3	0.7	0.402525	0.3	0.7	0.402528

Table 2. Numerical outcomes for Nusselt number.

Δ	Sc	Sh_x^{28}	Δ	Sc	Sh_x
0.3	0.3	0.265463	0.3	0.3	0.265471
0.4	0.3	0.264059	0.4	0.3	0.264066
0.5	0.3	0.262655	0.5	0.3	0.262663
0.3	0.3	0.265463	0.3	0.3	0.265471
0.3	0.4	0.266868	0.3	0.4	0.266878
0.3	0.5	0.268272	0.3	0.5	0.268280

Table 3. Numerical outcomes for Sherwood number.

η	PCM $f'(\eta)$	bvp4c $f'(\eta)$	Absolute error
0.0	5.09×10^{-21}	0.000000	5.09×10^{-21}
0.1	0.059923	0.121043	4.2×10^{-7}
0.2	0.159901	0.211168	1.7×10^{-6}
0.3	0.259954	0.311364	3.7×10^{-6}
0.4	0.359994	0.411624	6.03×10^{-6}
0.5	0.459987	0.511937	9.2×10^{-6}
0.6	0.559998	0.612295	1.4×10^{-5}
0.7	0.659935	0.713689	1.7×10^{-5}
0.8	0.759957	0.813110	2.3×10^{-5}
0.9	0.859902	0.913549	2.7×10^{-5}
10.0	0.959946	1.023997	2.8×10^{-5}

Table 4. Comparative analysis between bvp4c and PCM techniques for velocity.

η	PCM $\phi(\eta)$	bvp4c $\phi(\eta)$	Absolute error
0.0	1.000000091	1.000000	9.1×10^{-4}
0.1	0.8879855	0.903110	4.2×10^{-4}
0.2	0.709875	0.717920	7.04×10^{-4}
0.3	0.633047	0.641694	7.6×10^{-4}
0.4	0.568142	0.575623	6.4×10^{-4}
0.5	0.514767	0.519828	4.1×10^{-4}
0.6	0.472423	0.474360	1.9×10^{-4}
0.7	0.440544	0.439201	1.3×10^{-4}
0.8	0.418529	0.414291	3.2×10^{-4}
0.9	0.405765	0.489496	5.2×10^{-4}
10.0	0.401644	0.483614	6.03×10^{-4}

Table 5. Comparison between PCM and bvp4c techniques for concentration.

Received: 28 September 2021; Accepted: 18 January 2022
Published online: 15 February 2022

References

1. Abidi, A. & Borjini, M. N. Effects of microstructure on three-dimensional double-diffusive natural convection flow of micropolar fluid. *Heat Transfer Eng.* **41**, 361–376 (2020).
2. Siddiqa, S. *et al.* Effect of thermal radiation on conjugate natural convection flow of a micropolar fluid along a vertical surface. *Comput. Math. Appl.* **83**, 74–83 (2021).
3. Anwar, S. *Encyclopedia of Energy Engineering and Technology*; CRC Press: 2015.
4. Khoshvaght-Aliabadi, M., Sahamiyan, M., Hesampour, M. & Sartipzadeh, O. Experimental study on cooling performance of sinusoidal-wavy minichannel heat sink. *Appl. Therm. Eng.* **92**, 50–61 (2016).
5. Eringen, A. C. Theory of thermomicrofluids. *J. Math. Anal. Appl.* **38**, 480–496 (1972).
6. Stokes, V. K. *Micropolar Fluids* 150–178 (Springer, 1984).
7. Abo-Eldahab, E. M. Radiation effect on heat transfer in an electrically conducting fluid at a stretching surface with a uniform free stream. *J. Phys. D Appl. Phys.* **33**, 3180 (2000).

8. Abo-Eldahab, E. M. & Ghonaim, A. F. Radiation effect on heat transfer of a micropolar fluid through a porous medium. *Appl. Math. Comput.* **169**, 500–510 (2005).
9. Ramesh, G. K., Madhukesh, J. K., Prasannakumara, B. C., & Roopa, G. S. (2021). Significance of aluminium alloys particle flow through a parallel plates with activation energy and chemical reaction. *J. Therm. Anal. Calorim.*, 1–11.
10. Reddy, K. R. & Raju, G. Thermal effects in Stokes' second problem for unsteady micropolar fluid flow through a porous medium. *Int. J. Dyn. Fluids* **7**, 89–100 (2011).
11. Jyothi, A. M., Varun Kumar, R. S., Madhukesh, J. K., Prasannakumara, B. C. & Ramesh, G. K. Squeezing flow of Casson hybrid nanofluid between parallel plates with a heat source or sink and thermophoretic particle deposition. *Heat Transf.* **50**(7), 7139–7156 (2021).
12. Kumar, K. G., Gireesha, B. J., Ramesh, G. K. & Rudraswamy, N. G. Double-diffusive free convective flow of Maxwell nanofluid past a stretching sheet with nonlinear thermal radiation. *J. Nanofluids* **7**(3), 499–508 (2018).
13. Soundalgekar, V. & Takhar, H. Flow of micropolar fluid past a continuously moving plate. *Int. J. Eng. Sci.* **21**, 961–965 (1983).
14. Gorla, R. S. R. Mixed convection in a micropolar fluid from a vertical surface with uniform heat flux. *Int. J. Eng. Sci.* **30**, 349–358 (1992).
15. Rees, D. A. S. & Pop, I. Free convection boundary-layer flow of a micropolar fluid from a vertical flat plate. *IMA J. Appl. Math.* **61**, 179–197 (1998).
16. Gireesha, B. J., & Ramesh, G. K. (2018). Thermal analysis of generalized Burgers nanofluid over a stretching sheet with nonlinear radiation and non-uniform heat source/sink. *Arch. Thermodyn.*
17. Ramesh, G. K. & Gireesha, B. J. Flow over a stretching sheet in a dusty fluid with radiation effect. *J. Heat Transf.* **135**(10), 1 (2013).
18. Ganji, D. D., Sabzehmeidani, Y. & Sedighiamiri, A. *Nonlinear systems in heat transfer* (Elsevier, 2018).
19. Mahanthesh, B. & Mackolil, J. Flow of nanoliquid past a vertical plate with novel quadratic thermal radiation and quadratic Boussinesq approximation: Sensitivity analysis. *Int. Commun. Heat Mass Transf.* **120**, 105040 (2021).
20. Kumar, M. A., Reddy, Y. D., Rao, V. S. & Goud, B. S. Thermal radiation impact on MHD heat transfer natural convective nano fluid flow over an impulsively started vertical plate. *Case Stud. Therm. Eng.* **24**, 1026 (2021).
21. Khader, M. M. & Sharma, R. P. Evaluating the unsteady MHD micropolar fluid flow past stretching/shirking sheet with heat source and thermal radiation: Implementing fourth order predictor–corrector FDM. *Math. Comput. Simul.* **181**, 333–350 (2021).
22. Patil, A. A Modification and Application of Parametric Continuation Method to Variety of Nonlinear Boundary Value Problems in Applied Mechanics. 2016.
23. Shuaib, M., Shah, R. A. & Bilal, M. Variable thickness flow over a rotating disk under the influence of variable magnetic field: An application to parametric continuation method. *Adv. Mech. Eng.* **12**, 1687814020936385 (2020).
24. Shuaib, M., Shah, R. A., Durrani, I. & Bilal, M. Electrokinetic viscous rotating disk flow of Poisson-Nernst-Planck equation for ion transport. *J. Mol. Liq.* **313**, 11341 (2020).
25. Dombovari, Z. *et al.* Experimental observations on unsafe zones in milling processes. *Phil. Trans. R. Soc. A* **377**, 20180125 (2019).
26. Ali, V. *et al.* Thin film flow of micropolar fluid in a permeable medium. *Coatings* **9**(2), 98 (2019).
27. Rashidi, M. M. & Abbasbandy, S. Analytic approximate solutions for heat transfer of a micropolar fluid through a porous medium with radiation. *Commun. Nonlinear Sci. Numer. Simul.* **16**(4), 1874–1889 (2011).
28. Khan, W. *et al.* Thin film Williamson nanofluid flow with varying viscosity and thermal conductivity on a time-dependent stretching sheet. *Appl. Sci.* **6**(11), 334 (2016).
29. Khan, M. I., Waqas, M., Hayat, T. & Alsaedi, A. Soret and Dufour effects in stretching flow of Jeffrey fluid subject to Newtonian heat and mass conditions. *Results in physics* **7**, 4183–4188 (2017).

Acknowledgements

The authors acknowledge the financial support provided by the Center of Excellence in Theoretical and Computational Science (TaCS-CoE), KMUTT. Moreover, this research was funded by National Science, Research and Innovation Fund (NSRF), and Rajamangala University of Technology Thanyaburi (RMUTT) with Contract no. FRB65E0633M.2.

Author contributions

M.B., A.S., and T.G. modeled and solved the problem. M.B. and A.S. wrote the manuscript. S.M., T.G., P.K. and W.K. contributed in the numerical computations and plotting the graphical results. M.B., S.M. and T.G. work in the revision of the manuscript. All the corresponding authors finalized the manuscript after its internal evaluation.

Competing interests

The authors declare no competing interests.

Additional information

Correspondence and requests for materials should be addressed to W.K. or P.K.

Reprints and permissions information is available at www.nature.com/reprints.

Publisher's note Springer Nature remains neutral with regard to jurisdictional claims in published maps and institutional affiliations.



Open Access This article is licensed under a Creative Commons Attribution 4.0 International License, which permits use, sharing, adaptation, distribution and reproduction in any medium or format, as long as you give appropriate credit to the original author(s) and the source, provide a link to the Creative Commons licence, and indicate if changes were made. The images or other third party material in this article are included in the article's Creative Commons licence, unless indicated otherwise in a credit line to the material. If material is not included in the article's Creative Commons licence and your intended use is not permitted by statutory regulation or exceeds the permitted use, you will need to obtain permission directly from the copyright holder. To view a copy of this licence, visit <http://creativecommons.org/licenses/by/4.0/>.

© The Author(s) 2022